IOP Publishing Plasma Physics and Controlled Fusion
Plasma Phys. Control. Fusion **57** (2015) 014015 (10pp) doi:10.1088/0741-3335/57/1/014015

The physics and detection of nanodust in the solar system

N Meyer-Vernet[1], I Mann[2,3], G Le Chat[1], P Schippers[1], S Belheouane[1], K Issautier[1], A Lecacheux[1], M Maksimovic[1], F Pantellini[1] and A Zaslavsky[1]

[1] LESIA, Observatoire de Paris, CNRS, UPMC, Université Paris Diderot, Meudon, France
[2] EISCAT Scientific Association, Rymdcampus 1, 98192, Kiruna, Sweden
[3] Physics Department, Förvaltningshuset, Umea University 16, 90187, Sweden

E-mail: nicole.meyer@obspm.fr

Received 12 June 2014, revised 12 September 2014
Accepted for publication 19 September 2014
Published 28 November 2014

Abstract
The mass distribution of small bodies in the solar system extends over more than 35 orders of magnitude, from asteroids to nanodust, which bridge the gap between molecules and macroscopic submicron grains. The small size of nanograins compared to the relevant basic scales gives them peculiar properties. Some of these properties affect their electric charging and their large charge-to-mass ratio drives their acceleration to very high speeds in moving magnetised plasmas, as the solar wind and rotating planetary magnetospheres. The electric charge and/or high speed of nanograins have enabled them to be detected serendipitously in various parts of the solar system by several instruments designed to study larger dust, plasma particles, or waves, on a number of spacecraft. These discoveries have opened an emerging field of research, in which many open questions remain, in particular concerning the lower size limit of the particles.

Keywords: nanodust, solar system, interplanetary physics, space research instruments, solar wind, magnetospheres, nanograins

(Some figures may appear in colour only in the online journal)

1. Introduction

According to the International Council of Chemical Associations, a nano-object is defined as having at least one external dimension between 1 nm and 100 nm (norm ISO TS 27687). For compact spheres, this corresponds typically to a few tens to a few 10^7 atoms or small molecules (figure 1), so that nanodust lies at the frontier between macromolecules and bulk matter. This emerging field of research on nano-objects includes a various fauna, which is much more actively studied in the contexts of biology and nanotechnology than in astronomy and geophysics.

Nanodust has been inferred a long time ago in the interstellar medium [1]. It is revealed there by a variety of observed phenomena: optical luminescence, near- and mid-infrared continuum emission and spectral bands, microwave emission and far ultra-violet extinction [2]. The presence of nanodust outside the solar system is also inferred from the identification of presolar nanograins embedded in primitive meteorites [3] and in collected micro dust [4].

However, these grains cannot enter the solar system, as explained in section 4. Furthermore, the phenomena revealing nanodust in interstellar space are not likely to be observed in the solar system [2], mainly due to the small integrated depth involved, so that remote nanodust observations [5] are rare and nanodust detection is generally performed *in situ*. In the absence of dedicated instruments in operation, nanodust has thus been observed only recently in the solar system. It has been discovered in media as diverse as the solar wind [6] and cometary [7] and planetary environments (e.g. [8]). These discoveries were serendipitous, with some of them using instruments that were not designed to measure dust, but plasma particles or waves (e.g. [9]). Most of these detections were made possible by the high speed of nanoparticles, produced by acceleration by ambient moving magnetized plasmas: the solar wind [10] and/or rotating planetary magnetospheres [11].

Section 2 addresses small size effects, some of which affect the electric charge and increase its relevance. Section 3 studies the electric charge itself, which drives the high speed

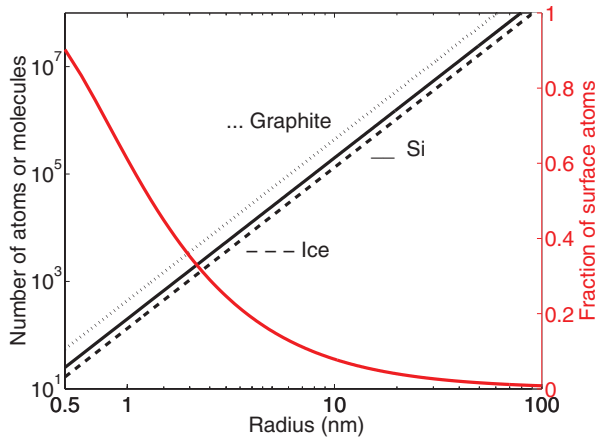

Figure 1. Number of atoms or molecules (black, left axis) and fraction of atoms or molecules located at the grain's surface (red, right axis) as a function of particle radius for compact spheres.

addressed in section 4. Finally, section 5 reviews nanodust detection, which was made possible by these latter effects.

2. What makes nanodust different?

First of all, nanodust has a large surface-to-volume ratio. Other differences arise when the particles' size is smaller than the basic scales determining their behaviour in relation to radiation and/or the ambient plasma. Further differences arise because of the strong increase of electric charging effects as size decreases.

2.1. Large surface-to-volume ratio

The surface-to-volume ratio varies in the inverse proportion of size for 3D compact particles and still faster for lower dimensional ones, including those having a fractal structure (e.g. [13]). Thus a large proportion of atoms are lying at the grain's surface (see e.g. [12] and figure 1). Surface atoms have too few bonding partners, yielding free radicals that produce chemical activity at the surface, surface reconstruction and coagulation (e.g. [14]), as well as changes in optical properties. Furthermore, the mean-square displacements of surface atoms are greater than within the grain, making the melting point and latent heat decrease and the diffusion coefficient in the grain increase [12].

2.2. Size smaller than de Broglie wavelengh: quantum confinement

From the Heisenberg uncertainty principle, confinement within a nanograin introduces an uncertainty in momentum, which plays an important role when the confinement energy becomes comparable to the thermal energy. Equivalently, the de Broglie wavelength $\hbar/mv$ of an elementary particle of mass m and speed v sets the scale below which quantum effects become conspicuous. Since electrons (of mass m_e) at temperature T have a thermal speed $\sim(k_BT/m_e)^{1/2}$ (k_B is Boltzmann's constant), one expects changes in radiating properties of semiconductors at sizes $\lesssim\hbar/(m_ek_BT)^{1/2}$. Since this is below the nanodust range for $T > 300$ K, quantum confinement effects are expected to be minor for solar system nanodust, although they are conspicuous in the cold interstellar medium [15].

2.3. Size smaller than mean electron free paths

The mean free path of electrons l_e in most materials increases with energy above a few 100 eV and has a minimum $\lesssim$1 nm near tens of eV. Still below this energy, it increases as energy decreases up to $l_e \gtrsim 1$ nm near 1 eV [16].

This has important consequences for the electric charging of nanograins of size $\lesssim l_e$ in plasmas: the sticking coefficient of the plasma electrons impacting the grain decreases below unity [17–19], and the electron secondary emission induced by impacting electrons exceeds the value for bulk matter [20, 21].

2.4. Size smaller than scales relevant for ambient radiation

The attenuation length of photons producing photoelectron emission in most materials ($\sim$ 10–100 nm) largely exceeds the photoelectron escape length ($l_e \sim$ 0.5–5 nm) [22]. Therefore, for nanograins of radius $a \lesssim l_e$, the photoelectrons have a better chance to escape than from bulk matter, which increases the photoelectron emission yield—i.e. the number of ejected photoelectrons per absorbed photon [22, 23]. This effect can be counterbalanced by two further effects. First, the removal energy of an electron increases for very small grains since the image charge contribution $\sim (3/8)(e^2/4\pi\epsilon_0 a)$ adds to the work function [24]; this increases the photon energy required for photoelectron emission. Second, the wavelength of radiation mainly responsible for ionization $\lambda \sim hc/E_{\rm Bohr} \sim 0.1$ μm ($E_{\rm Bohr} \simeq 10$ eV is the Bohr energy) exceeds the nanodust size; hence the photon absorption cross-section is expected to decrease with grain size in proportion of a^3 (Rayleigh *oblige*), i.e. faster than the a^2 variation of the grain's cross-sectional area. The final result depends on the grain size and material and on the ambient radiation.

Finally, the heat capacity of a nanograin can become so small that the absorption of a single photon changes significantly its temperature. This stochastic heating affects the radiating properties of interstellar grains (see e.g. [25]), but this is not so in the solar system because the intense solar radiation field produces a photon impact rate exceeding the grain's heating rate (except below the nanometer size) [2].

2.5. Size smaller than the plasma Landau radius

In a plasma of temperature T, the so-called plasma Landau radius

$$r_{\rm L} = e^2/(4\pi\epsilon_0 k_B T) \qquad (1)$$

is the distance below which the mutual electrostatic energy of two approaching particles of charge $\pm e$ exceeds the kinetic energy of their relative motion, so that they significantly perturb each other's trajectories. This scale determines the plasma particle cross-section for Coulomb collisions producing large

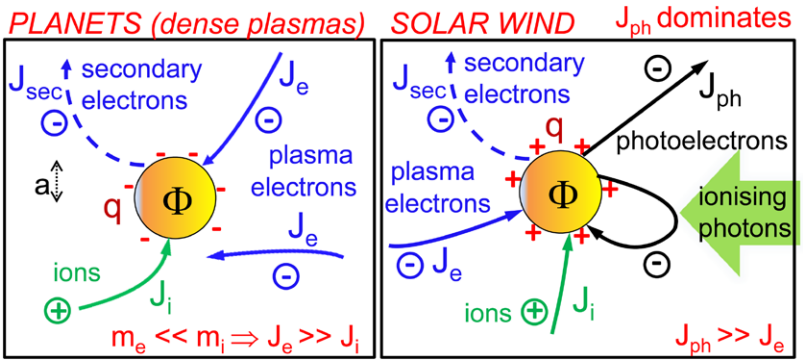

Figure 2. Basics of grain charging.

perturbations. It is also of major importance for dust grains since the plasma particles approaching a grain of radius $a \lesssim r_L$ induce polarization charges whose Coulomb attraction increases significantly the collected fluxes and thus modifies the grain charging (section 3.2). Furthermore, at this scale the charging becomes discretized [26] (section 3.2).

Since (1) can be written

$$r_{L(nm)} \simeq 1.44 / T_{eV} \tag{2}$$

these effects hold in cold plasmas, as the Earth's low ionosphere (see e.g. [27, 28]), the interstellar medium (see e.g. [29]) and the environment of outer planet satellites [26].

2.6. Nucleation on charged nanograins

The grain's electric charge (section 3) can affect its size via growth and/or disruption. Consider the growth via nucleation of water molecules on ice grains [30]. It is governed by the tendency of the system to minimize the Gibbs free energy, given for an uncharged grain by $G = 4\pi\, a^2\, \sigma - N\, k_B T \ln S$ in the framework of liquid drop theory; here the first term is the surface energy ($\sigma \sim 0.1$ J m^{-2}); the second term represents the energetic preference for condensation, $N \propto a^3$ being the number of grain's molecules and S the supersaturation ratio (vapour pressure divided by saturation pressure). The first term produces an energy barrier which prevents nucleation on uncharged grains of size smaller than about 1 nm at $T \simeq 130$ K in the Earth thermosphere. The grains' electric charge changes this situation since it (Coulomb) attracts the incident dipolar water molecules, which decreases the Gibbs energy and suppresses the energy barrier for $T \leqslant 130$ K [31]. This enables the numerous subnanometer charged 'smoke' particles present in the thermosphere to act as condensation nuclei, therefore increasing by a large amount the formation of nanodust in this region [18] (see section 5.1).

2.7. Electrostatic and centrifugal disruption

The electrostatic field E at the surface of a nanograin of radius a and charge q increases in proportion of q/a^2; since q varies in proportion of a or less (section 3.2), E can become very high for nanograins. When the electrostatic stress ($\propto E^2$) exceeds the maximum grain's tensile strength against fracture S, it makes the grain explode (e.g. [20, 32]), so that the minimum size of a grain carrying Z elementary charges is [34]

$$a_{nm} \simeq 0.4 Z^{1/2} (S / 10^9 \mathrm{Nm}^{-2})^{-1/4} \tag{3}$$

where we have normalized the maximum nano grain tensile strength S to the typical value for polycrystalline matter or tektites. This limit should be considered together with field emission; for example, for compact ice grains carrying one electron in Enceladus plume (not less because $a \lesssim r_L$ and not more because of field emission, see section 3.2), (3) yields a minimum diameter of 1.4 nm [26].

Another size limitation can be produced by the centrifugal stress due to the grain's spin induced by impacts of ambient particles [20, 33]. Contrary to the electrostatic limit, it concerns also uncharged grains. When the grain is charged and the time scales for the grain to be charged and to spin up are both smaller than the other relevant time scales, both effects can act simultaneously. In that case the grain minimum size is determined by the largest of both minima, which is set by centrifugal disruption if the temperature of the species making the grain spin satisfies $T_{eV} > (S/10^9\ \mathrm{Nm}^{-2})^{1/4}$. This is so for fragile grains, or warm media as for example the innermost interplanetary medium [35]. The minimum radius is then given by $a_{nm} \simeq 0.5 \times T_{eV}^{1/3} (S / 10^9 \mathrm{Nm}^{-2})^{-1/3}$ (e.g. [34]) instead of (3).

3. How are nanograins charged in solar system plasmas?

3.1. Basics of electric charging

Dust grains charge by collecting and emitting charged particles, which changes their charge and electrostatic potential, which in turn changes the fluxes of incoming and outgoing charged particles, until an equilibrium is reached when the electric currents balance (see e.g. [36]).

In dense plasmas (figure 2, left), as in planetary ionospheres and the inner magnetospheres of outer planets, the photoelectron current is generally negligible. The plasma electron current largely exceeds the ion current because of the smaller electron mass (since both species generally have temperatures of the same order of magnitude), so that the grain charges negatively. This negative charge repels the incoming electrons and an equilibrium is reached when the grain's charge repels

sufficiently the electrons so that their collected current balances that of the positive ions. For doing so, the grain's electrostatic potential Φ with respect to the ambient plasma must ensure that the potential energy $-e\Phi$ equals a few times the kinetic energy of the plasma electrons. This yields $-e\Phi \simeq \eta\, k_B T$, where η equals a few units. A roughly spherical grain of radius a much smaller than both the plasma Debye length L_D and the grains' separation carries the electric charge $q \simeq 4\pi\, \epsilon_0 a\, \Phi$. Substituting the above value of Φ and using (1) yields the normalized grain charge q/e at equilibrium

$$Z = -\eta a / r_L \tag{4}$$

where η—of order of magnitude unity, can be calculated straightforwardly since the small size of the grain ensures that the particles are subjected to its Coulomb potential without intervening barriers of potential (the so-called orbit-limited condition, see e.g. [37]). In a Maxwellian plasma with one singly charged ion species of the same concentration and temperature as electrons and a sticking coefficient $\simeq 1$, we have $\eta \simeq 2.5 - 3.9$ for ion mass $m_i \simeq m_p - 30\, m_p$, m_p being the proton mass [36].

In contrast, in the interplanetary medium and in dilute regions of planetary magnetospheres, the charge flux is generally dominated by photoemission produced by solar photons of energy exceeding the work function of the grain material (figure 2, right). The grain thus charges positively until its positive charge binds sufficiently the photoelectrons to reduce their escaping flux so that it balances the flux of incoming plasma electrons. For doing so, the grain's electric potential must provide the photoelectrons with a potential energy $-e\Phi$ equal to a few times their typical kinetic energy. Since for most materials exposed to the solar flux, the photoelectron velocity distribution can be approximated by a Maxwellian (of temperature T_{ph}) [38], one has $e\Phi = +\ \eta\, k_B T_{ph}$ with η equal to a few units. Therefore, a sunlit grain carries a number of charge units

$$Z = +\eta a / r_L \tag{5}$$

where r_L is given by substituting in (1) the effective photoelectron temperature of a few 10^4 K (in practice 1–4 eV).

These basic results can be modified by two effects. First, incident electrons of energy exceeding the typical atomic binding energy $E_{Bohr} \simeq 10$ eV can produce secondary electron emission. In addition to shifting the grain electric potential to more positive values, this effect can produce two stable equilibrium charges of opposite signs for a given grain in a given environment when the ambient electron velocity distribution is not Maxwellian [39]. Second, when the dust concentration is so high that the grains' Debye spheres overlap, the electrons are depleted with respect to the ions since many of them rest on the grains' surface, which in turn reduces the grains' charge [26, 36, 40–42].

3.2. Electric charging of nanodust

How does nanodust charging differ from this picture? First, as noted in section 2.5, when the grain radius is of order the Landau radius (1) or smaller, the polarization induced on a grain by approaching charges produces an electric potential that perturbs significantly their trajectories and modifies the charging currents. This polarization increases significantly the flux of particles whatever the grain charge (see e.g. [29]). Since the flux of repelled particles increases more than the other ones, this effect tends to make the negative charge more negative [26]. Such phenomena affect noctilucent cloud particles and meteoritic dust (see e.g. [28]) as well as nanograins in Enceladus plume [26] (section 5.1).

Second, one sees from (4)–(5) that $|Z|$ is not large when $a \lesssim r_L$, so that a statistical treatment is needed. In that case, one must calculate the probability $f(Z)$ that a grain carry the electric charge Ze. In the simple case when the charging currents come from the ambient electrons (J_e) and ions (J_i) in stationary conditions, the probability can be deduced from the recurrence relation $f(Z)/f(Z+1) = J_e(Z+1)/J_i(Z)$ [29]. However, because of the small surface area, the charging time scale is large, so that nanograins may not carry their equilibrium charge; in that case, the problem must be solved numerically (see e.g. [43]).

Finally, for nanograins we have $e^2/4\pi\, \epsilon_0 a \simeq 1.4$ eV, so that the surface Coulomb electric field deforms significantly the potential barrier at the surface, which enables electrons inside to tunnel efficiently. In practice, this process becomes efficient when the (inward) electric field exceeds 10^9 V m^{-1}. An ejected electron near the surface of a grain of charge $Ze < 0$ will be subjected to the field amplitude $|E| \simeq (Z+1)e/4\pi\, \epsilon_0 a^2$. Hence electron field emission limits the grain charge to $|Z| < (1 + 0.7 a_{nm}^2)$ (e.g. [29, 44]). Note that ion field emission, which limits the positive charging, is generally negligible because it requires a much higher electric field.

In summary, when the grain's size is of order r_L or smaller, the equilibrium charge no longer decreases in proportion of the size, but remains comparable to one electron charge in a wide range of sizes, mainly because the probability that an uncharged grain collects an electron far exceeds the probability that a neutral or negatively charged grain collects an ion. This charging is crucial for their detection by plasma analyzers (section 5.1) and for their dynamics, which is addressed below.

4. Dynamics of nanodust in solar system plasmas

With the electric charge decreasing in proportion of the grain's radius a or less, the charge-to-mass ratio q/m of nanograins becomes fairly high and so does the acceleration by the Lorentz force, with major consequences on the dynamics in magnetized plasmas. Let us estimate q/m. In basic units, we have in order of magnitude $m/m_p \sim (a/r_B)^3$ for compact grains and $|q/e| \sim 1 + \eta\, a/r_L$ [26], where η equals a few units (section 3.1), $r_B \simeq 0.05$ nm is the Bohr radius and r_L the Landau radius of the charge species dominating the grain's charging. Hence, in terms of the grain size and plasma parameters

$$\begin{aligned} |q/m| &\gtrsim 3.5 \times 10^{-4} \times \left(e/m_p\right)/\left(r_{L(\mathrm{nm})}\, a_{nm}^2\right) \\ &\gtrsim 2.5 \times 10^{-4} \times \left(e/m_p\right) T_{\mathrm{eV}}/a_{nm}^2 \end{aligned} \tag{6}$$

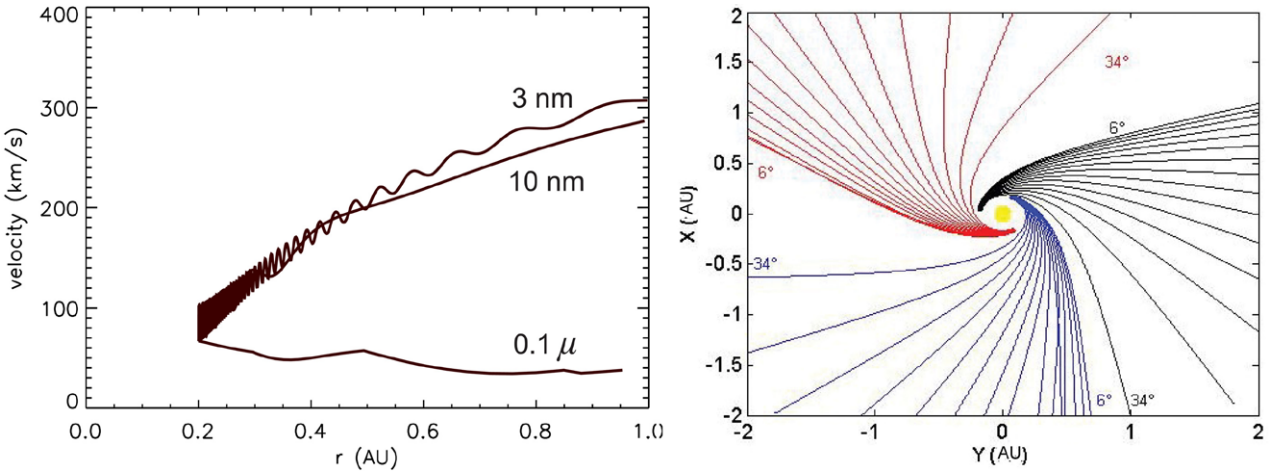

Figure 3. Speed of nanodust and 0.1 μm particles as a function of heliocentric distance, showing the nanodust accelerated at about 300 km s^{-1} at 1 AU (left, adapted from [49]). Trajectories of 3 nm radius particles projected on the solar magnetic equatorial plane for three initial longitudes and different initial latitudes (indicated on the figure), showing the particles tending to follow the solar wind spiral magnetic field lines (right, from [50]).

Consider first nanograins in the interstellar medium close to the heliosphere, of approximate radius 100 AU (1 AU $\simeq 1.5 \times 10^{11}$ m is the Sun–Earth distance). With a relative velocity $V \sim 25$ km s^{-1}, a plasma temperature $T \sim 0.5$ eV and magnetic field $B \sim 3 \times 10^{-10}$ T (e.g. [45]), (6) yields a gyroradius $r_{\rm gyr} \sim mV/qB \sim 0.05 a_{nm}^2$ AU. Thus $r_{\rm gyr} < 100$ AU for $a < 50$ nm. Hence grains of this size are deflected and interstellar nanograins, for which $r_{\rm gyr} \ll 100$ AU, follow the interstellar field lines and cannot enter the heliosphere (see e.g. [46]).

Now, consider the solar wind and the inner magnetospheres of outer planets, where the charging is dominated by respectively photoelectrons and plasma electrons, of energy around a few eV . From (2), $r_{\rm L}$ is in the nanometer range, so that (6) yields

$$|q/m| \sim \left(e/m_p\right) 10^{-3} / a_{nm}^2 \qquad (7)$$

and the Lorentz force generally dominates the other forces in magnetized plasmas.

4.1. Solar wind

To a first approximation, the solar wind plasma expands radially at a speed $V \simeq 400$ km s^{-1} and carries a magnetic field, which has a spiral shape due to the solar rotation at $\Omega \simeq 2.7 \times 10^{-6}$ rad s^{-1}. The ratio of azimuthal to radial magnetic components at heliocentric distance r is thus $\Omega r/V$ in the ecliptic plane where lie most solar system objects and the magnetic field radial component varies with distance as r^{-2}. The magnetic field modulus is $B \simeq 4.5 \times 10^{-9}$ T at $r \simeq 1$ AU where $\Omega r/V \simeq 1$ (see e.g. [47]).

We deduce from (7) that the angular gyrofrequency (normalized to Ω) of a nanograin of radius a and velocity v is $\omega_{\rm gyr}/\Omega = (qB/m)/\Omega \simeq 150/a_{\rm nm}^2$ at 1 AU, whereas its gyroradius (normalized to r) $r_{\rm gyr}/r \lesssim \left|(\mathbf{v}-\mathbf{V})_\perp\right| / (\omega_{\rm gyr} r) \simeq 0.5 \times 10^{-2} a_{\rm nm}^2$ at 1 AU (the subscript $\perp$ denotes the component $\perp \mathbf{B}$). Both quantities increase with distance inward of 1 AU, but the normalized gyroradius remains roughly constant farther out since the magnetic field there varies roughly as $1/r$.

Hence at any heliocentric distance a nanoparticle of radius <10 nm has a gyroradius smaller than the distance, so that it is quickly picked-up by the solar wind and accelerated roughly to the drift velocity, equal to the projection of the solar wind velocity normal to the magnetic field, which amounts to about 300 km s^{-1} at 1 AU [10] (figure 3). This holds provided that the nanoparticle is released farther than about 0.2 AU from the Sun; at closer distances, nanograins can be trapped by the combined actions of the solar gravitational attraction, the magnetic mirror force and the centrifugal force [48].

4.2. Rotating magnetospheres

Most solar system planets are rotating about an axis making a small angle with the normal to their orbit and have an intrinsic magnetic field. For the Earth and the giant outer planets Jupiter and Saturn, this field is roughly dipolar, with the magnetic dipole axis lying close to the spin axis Ω (see e.g. [47]).

Consider a planet of mass M, radius R and magnetic field amplitude B_R at equator. Assume a nanograin of charge q and velocity $\mathbf{v}$ at distance r, close to the equatorial plane where lie the satellites and other material, so that most grains are likely to be produced there. The plasma rotates with the azimuthal velocity $\boldsymbol{V}_{\rm rot} = \Omega \times \mathbf{r}$ and the Lorentz force $F_{\rm L} = q\,(\mathbf{v} - \boldsymbol{V}_{\rm rot}) \times \mathbf{B}$ is directed outwards for $q > 0$, farther than the corotation distance. It therefore tends to eject nanograins small enough for the corotation potential energy $\Phi_{\rm rot} \simeq q\Omega\, B_R R^3/r$ to exceed half the gravitational energy $\Phi_G/2 \simeq mMG/2r$; the grains released at radius r_0 are ejected with a speed v_{ej} approximately given by [11]

$$v_{ej}^2 \simeq (2MG/r_0)\,(\Phi_{\rm rot}/\Phi_G - 1/2) \qquad (8)$$

Note that grains of gyroradius smaller than the scale of magnetic field variation remain confined along the closed magnetic field lines, so that (8) does not hold for too small grains.

Nanograins produced by volcanoes of Jupiter's satellite Io are ejected in this way from Jupiter's magnetosphere at speeds of nearly 300 km s^{-1} if their size lies between a few nanometers to a few tens nanometers. Similarly, nanograins emerging from Saturn's icy moon Enceladus are ejected from Saturn's environment, albeit at somewhat smaller speeds due to the smaller rotation rate and magnetic field of Saturn (see e.g. [8]).

5. *In situ* detection of nanodust in solar system plasmas

5.1. Nanodust detection with dust and plasma analyzers

The presence of nanodust in the Earth lower ionosphere was inferred long ago (see e.g. [51] and references therein) from the observation of noctilucent ('night-luminous') clouds (NLC), which revealed the occasional presence of aerosol particles in the polar low ionosphere. And the ubiquitous presence of so-called meteor smoke particles produced by ablation and subsequent recondensation of meteoric matter was suggested a long time ago.

These inferences have been confirmed by *in situ* measurements (see e.g. [52]) and nanodust has been shown to play a major role in the physics of the Earth's polar mesosphere in summer at 80–90 km altitude, which is the coldest place on Earth. With a temperature <150 K, below the water frost point, large quantities of icy nanograins can be produced there by condensation of water vapour on meteor smoke (section 2.6). These nanograins are at the origin of three conspicuous phenomena. First, nanograins large enough to scatter visible light produce the above-mentioned NLC's (also known as Polar Mesospheric Clouds). Second, most nanograins are charged negatively (section 3.1) and since the Landau radius $r_L > 0.1$ μm at $T < 150$ K, most of them carry one electron (section 3.2) and act as sinks for ambient electrons, producing large decreases in plasma electron density. Third, the variations in plasma electron density strongly backscatter radio waves, producing Polar Mesosphere Summer Echoes [53].

At higher altitudes in the Earth environment, a flux of nanodust of radius $\lesssim 5$ nm (mass $\lesssim 10^{-21}$ kg) compatible with the interplanetary dust model at 1 AU (figure 4) has been measured by a penetration dust detector on the International Space Station in low Earth orbit; these particles may be either debris or interplanetary dust [54].

Farther out, the ion mass spectrometers on the spacecraft Vega's [55] and Giotto [7], designed to study the composition of cometary dust, detected unexpected signals at 10^6 km from the nucleus of comet Halley. These signals were first thought to be spurious noise because the instruments were not designed to operate with such small particles, but a detailed analysis has attributed these observations to nanodust of mass $\simeq 10^{-21}$ kg [7].

Nanodust has also been detected serendipitously in the environments of outer planets by instruments not designed to do so. A subsystem of the plasma spectrometer on Cassini, designed to measure electrons at Saturn, detected negatively charged particles of energy per charge corresponding to masses up to about 10^4 m_p and kinetic energy consistent with the spacecraft velocity, revealing large quantities of nanograins in Titan's atmosphere [56]. The mainly negative charge agrees with expectations (section 3.2), as well as do the grains' concentrations [57].

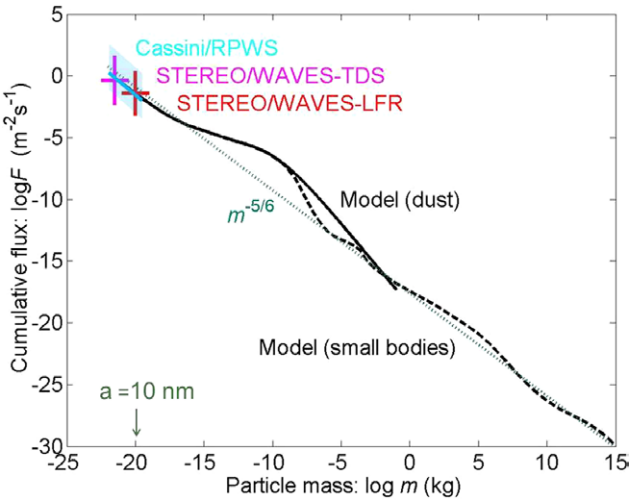

Figure 4. Cumulative flux of interplanetary dust and bodies near 1 AU from the Sun. The superposition of models for dust ([89], continuous line), small bodies ([90], dashed) and collisional equilibrium $\propto m^{-5/6}$ (dotted), is reproduced from [47], with measurements of nano dust by [6, 85, 86 and 87] superimposed.

Still in Saturn's environment, the same instrument also discovered a large concentration of negatively charged nanograins in the plume ejected by the geologically active icy moon Enceladus [58, 59]. The mainly negative charge and the minimum size of about 1 nm [59] are in agreement with expectations [26] (sections 2.7 and 3.2).

Nanodust was also detected serendipitously by instruments designed to measure dust grains of much larger size. In that case, the detection was made possible by the high speed of these particles (section 4.2). The dust analyzer onboard the spacecraft Ulysses detected 'small events' which were initially attributed to streams of ~0.2 μm grains coming from Jupiter at about 50 km s^{-1} [60]. Shortly after, these streams were recognized, from dynamics calculations, as made instead of nanodust $\sim 10^3$ less massive and moving ~5–10 times faster [61], well outside the calibration range of the instrument. These results have been confirmed and completed by observations from dust analyzers onboard the spacecraft Galileo and Cassini (see e.g. [8]) and by a wave instrument [62].

Similarly, the dust analyzer on Cassini has detected nanodust streams ejected from the Saturn environment and further accelerated by the solar wind [63]. As for Jupiter nanodust streams, these measurements were mainly based on dynamics calculations [8] (section 4) since the nanodust size and speed are outside the calibration range of the dust detector.

5.2. Nanodust detection with wave instruments

Wave instruments are routinely used in space for *in situ* plasma measurements via quasi-thermal noise spectroscopy [64]. This technique is based on the voltage fluctuations

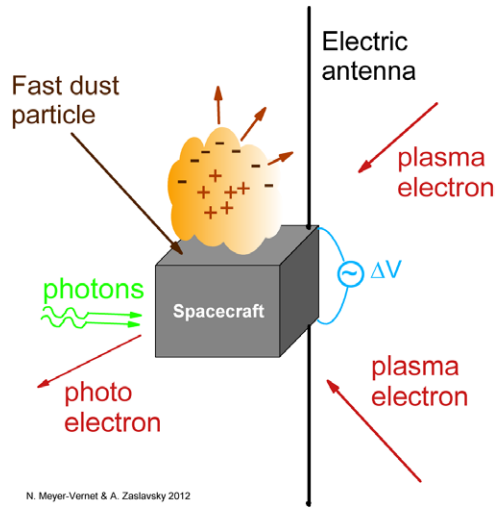

Figure 5. Principle of *in situ* measurements of plasma and dust via waves. Plasma particles passing-by the antennas (or impacting or being ejected) produce a quasi-thermal electrostatic noise whose power spectrum reveals plasma properties. Dust impacts at high speed produce partial ionisation of the dust and target, yielding an expanding plasma cloud. The cloud's charges produce voltage pulses whose analysis reveals some dust properties. Adapted from [9] with the kind permission of Springer Science and Business Media.

induced on electric antennas by the quasi-thermal motion of the ambient electrons and ions (figure 5) [65]. These fluctuations produce a peak in spectral density at the local plasma frequency, whose shape reveals the electron temperature and further plasma properties [66].

Charged dust grains passing closer than the Debye length ($\sim$ 10 m in the solar wind at 1 AU) from the electric antennas also produce electric voltage fluctuations, whose detection, however, requires very large grain sizes and/or number densities [67, 68]. In contrast, a dust grain impacting the spacecraft (or antennas) at a large speed produces a strong shock compression which vaporises and ionises the dust as well as a part of the impact crater. This produces an expanding plasma cloudlet whose residual ionisation exceeds by several orders of magnitude the initial grain charge and can be used to detect the grain (figure 5). This technique was pioneered when the spacecraft Voyager crossed the dusty rings of Saturn; at this occasion, the inboard radio [69] and plasma wave instruments [70] detected dust grains, opening the way to microdust measurements with wave instruments in various environments (see [68, 71, 72] and references therein).

The detection is based on the residual charge Q carried by the electrons and/or the ions of the impact cloudlet, which can be recollected by a biased target. A spacecraft in the solar wind is positively charged (section 3.1) and thus recollects the cloudlet's electrons [9, 73], making its floating potential change by $\simeq -Q/C_{SC}$(C_{SC} being the spacecraft capacitance), so that a monopole antenna (which measures the difference of potential between an antenna arm and the spacecraft) measures a voltage pulse

$$\delta V \simeq +\Gamma Q / C_{SC} \tag{9}$$

where Γ is the wave receiver gain. Modern wave instruments include two independent parts: a time domain sampler measuring the voltage as a function of time at a high rate and a frequency receiver measuring the time-integrated power spectrum. The individual voltage pulses produced by dust impacts can be detected by the time domain sampler, whereas the corresponding voltage power spectrum due to many impacts during the integration time can be detected by the frequency receiver of the instrument [74].

The impact charge Q depends on the grain mass m and speed v and this dependence is used by the classical impact ionisation dust detectors [75], with various relationships of the form $Q \propto m^{\alpha} v^{\beta}$ where $\alpha \simeq 1$ and $\beta \simeq 3 - 4.5$. The coefficients depend on mass, speed, angle of incidence, as well as grain and target composition [76, 77], and have not been measured for either nanodust or $v \gtrsim 70$ km s^{-1} [75]. Furthermore, the huge strain rate $v/a \simeq 3 \times 10^{13}$ s^{-1} for particles of radius $a \simeq 10$ nm impacting at $v \simeq 300$ km s^{-1} lies in a newly explored range of modelling (e.g. [78]), whereas existing N-body simulations [79] of the plasma cloud expansion corresponding to a fast nanodust impact only consider uncharged targets.

Nanodust detection was made possible by the high speed of nanodust together with the much faster increase of the impact charge with speed than with mass. Why does the impact charge increase much faster than the grain's kinetic energy? This is so because Q depends on vaporization and ionization, in a complex process involving plasma expansion and recombination. The grain speed determines not only the kinetic energy but also the time scale of the process, with incomplete recombination requiring short time scales. Indeed, for a grain of radius a and mass density ρ, the incident kinetic energy $\rho\,(4\pi\,a^3/3)v^2/2$ encounters a surface $\pi\,a^2$ of the target during the time $\sim a/v$, yielding the power flux $P \sim \rho\, v^3$. With $\rho \simeq 2.5 \times 10^3$ kg m^{-3} (typical for silicates) and $v \simeq 300$ km s^{-1}, this yields the huge power flux $W \sim 10^{20}$ W m^{-2}.

In the absence of laboratory calibrations or numerical simulations for impact ionization of high-speed nanodust, we have used the empirical relation [80, 81]

$$Q_{(\mathrm{Cb})} \simeq 0.7 m_{(\mathrm{kg})}^{1.02} v_{(\mathrm{kms^{-1}})}^{3.48} \tag{10}$$

whose application to fast nanodust is consistent with independent results as explained below. According to (10), a 10 nm grain impacting at 300 km s^{-1} should produce a similar impact ionisation charge as a grain more massive by 3 orders of magnitude but less fast by a factor $\sim$7. Even though this relationship was not calibrated for nanodust, it is remarkable that the initial (incorrect) identification of Jovian dust streams by traditional dust detectors based on calibrations [60] and the final (correct) identification based on dynamics (grains of mass smaller by 3 orders of magnitude but moving 5–10 times faster [61]), have similar values of the quantity $mv^{3.5}$. This suggests that this calibration holds also approximately for fast nanodust. Note also that impact ionisation yields of materials relevant for the STEREO and Cassini spacecraft have been reported recently for microdust at speeds below 40 km s^{-1} [82]. Extrapolating these results for nanodust impacting at 300 km s^{-1} produces charges of the same order of magnitude as those given by (10). We estimate that using (10) for fast nanodust introduces an uncertainty of about a factor of ten.

The measurement of the power spectrum due to the pulses of amplitude (9) with the calibration (10) has enabled us to detect Jovian nanodust streams with the Cassini/RPWS low-frequency receiver [62], simultaneously to the detection of these particles by the Cosmic Dust Analyser onboard the spacecraft Cassini and Galileo [83].

The serendipitous discovery of fast nanodust in the solar wind at 1 AU [6] by the frequency receiver of the instrument STEREO/WAVES, designed to study solar radio emissions, came as a surprise because the detection was not made by traditional dust detectors. This detection should not, however, have been surprising since (i) the production of such particles in the inner heliosphere by collisional fragmentation of larger dust and their acceleration to high speeds was suggested a few years before [84], (ii) the flux detected was compatible with the extrapolated interplanetary dust model [89] and (iii) the detection via impacts on the spacecraft surface is much more sensitive than traditional dust detectors since the collecting area and solid angle are larger by several orders of magnitude.

The STEREO discovery was confirmed by detailed studies of the data from the two independent parts of the WAVES instrument: the low frequency receiver [86] and the time domain sampler [85], as well as onboard another spacecraft: Cassini [87]. Indeed, during the one month period when the Cassini/RPWS instrument was turned on near 1 AU before reaching Jupiter and Saturn, the low-frequency receiver (using the antennas in monopole mode) was able to measure the power spectrum produced by the pulses given by (9) with a flux compatible with the STEREO measurements [87] (figure 4).

It is important to note that the dust detection via recollection of the impact charges by the spacecraft requires the antennas to be used in monopole mode in order for them to detect the pulses in spacecraft potential [72]. Unfortunately, many wave instruments use instead the antennas as dipoles, which measure the voltage between two antenna arms, because this provides a greater sensitivity and a better calibration.

In that case, the antennas can still detect voltage pulses produced by dust impacts—albeit by other mechanisms. First, if the antennas have a large surface area, they can collect some of the charges produced by impacts on the spacecraft or on their own surface. Second, the ions of the impact plasma cloud (remaining after recollection of the electrons by the positively charged spacecraft) can produce a voltage perturbation on an antenna close to the impact site, which is generally much smaller than (9) and in practice only detectable for large grains [72], except when these impact charges close to an antenna can perturb the photoelectron sheath surrounding it, in which case they can produce large voltage pulses, as was observed on STEREO [73, 85, 88].

Indeed, because of the intense solar radiation, a body in the solar wind tends to eject much more photoelectrons than it collects ambient electrons (section 3); equilibrium therefore requires that most photoelectrons remain trapped by the (positive) body's potential, producing a photoelectron sheath around it, of radius roughly the photoelectron Debye length ($L_{\rm Dph} \sim 0.5$ m at 1 AU). As photoelectrons move outwards from the surface of an antenna of radius $r_a \ll L_{\rm Dph}$ along their balistic orbits in the photoelectron sheath, their transverse energy decreases rapidly (conservation of angular momentum *oblige*). Hence the electric field perturbation produced by the dust impact charges is sufficient to eject the photoelectrons from their trapped trajectories. This interrupts momentarily the photoelectron return current on a fraction l/L of the antenna, producing a voltage pulse [73, 88]

$$\delta V_{\rm ph} \simeq \Gamma\left(k_{\rm B}T_{\rm ph}/e\right)(l/L) \tag{11}$$

This latter mechanism, which affects only one antenna arm and thus produces a pulse detected both in monopole and dipole mode, requires two conditions to operate: first, an adequate antenna geometry, as is the case for the STEREO antennas lying close to the spacecraft (which has plane faces), in contrast to other interplanetary probes carrying wave instruments; second, the antenna radius must be large enough for the interruption of the photoelectron current to produce a detectable voltage pulse [88].

The interplanetary nanodust fluxes detected near 1 AU on STEREO/WAVES [6, 85, 86] and Cassini/RPWS [87] by these mechanisms are shown in figure 4, superimposed to the flux models for interplanetary dust [89] and small bodies [90]. Both STEREO and Cassini measured large variations in flux—reaching two orders of magnitude, at several time scales. This is not surprising, given the expected variations in nanodust production [92] and the ubiquitous fluctuations in the solar wind properties that determine the Lorentz force governing nanodust dynamics [10, 36, 48, 91].

6. What next?

Most nanodust detections in the solar system were performed by instruments not designed to do so; in particular, neither the cosmic dust analyzers nor the wave instruments onboard solar system space probes in operation are calibrated for nanodust detection. Hence several major questions about these particles are still pending. Among them are the composition, physical state and lower size limit of interplanetary nanodust. The composition of nanodust streams coming from the environments of Jupiter [93] and Saturn [63] have been studied in detail (see e.g. [8]); the size distribution of the smaller nanodust in Titan's ionosphere (see e.g. [57]) and in the Enceladus plume have also been measured [59] and found to agree with the size limitations discussed in section 2.7 [26]. But this is not so for the interplanetary nanodust, for which there is presently no dedicated detector in operation, although such an instrument is being developed [94]. In particular, the smallest size is presently unknown, even though we can derive an educated guess for electrostatic disruption of nanograins charged by photoelectron emission near 1 AU, using (3), (5) and (2): for an interplanetary grain of tensile strength S, the minimum radius is expected to be $a_{\rm min} \simeq (0.5-1)(S/10^9\ {\rm N\ m^{-2}})^{-1/2}$ nm.

Acknowledgments

NM-V thanks the ISSI International team on 'Nanodust in the Solar System' for useful discussions on nanodust and the International Space Science Institute for having fostered them.

References

[1] Platt J R 1956 *Astrophys. J.* **123** 486–90
[2] Li A and Mann I 2012 *Nanodust in the Solar System: Discoveries and Interpretations* (*Astrophysics and Space Science Library*) vol 385, ed Mann I *et al* (Heidelberg: Springer) pp 5–30
[3] Lodders K 2005 *Chem. Erde: Geochem.* **65** 93
[4] Bernatowicz T J *et al* 1991 *Astrophys. J.* **373** L73
[5] Hervig M E *et al* 2009 *Geophys. Res. Lett.* **36** L18805
[6] Meyer-Vernet N *et al* 2009 *Solar Phys.* **256** 463–74
[7] Utterback N G and Kissel J 1990 *Astron. J.* **100** 1315–22
[8] Hsu H-W, Krüger H and Postberg F 2012 *Nanodust in the Solar System: Discoveries and Interpretations* (*Astrophysics and Space Science Library*) vol 385, ed Mann I *et al* (Heidelberg: Springer) pp 77–117
[9] Meyer-Vernet N and Zaslavsky A 2012 *Nanodust in the Solar System: Discoveries and Interpretations* (*Astrophysics and Space Science Library*) vol 385, ed Mann I *et al* (Heidelberg: Springer) pp 133–60
[10] Czechowski A and Mann I 2010 *Astrophys. J.* **714** 89–99
[11] Burns J A, Hamilton D P and Showalter M R 2001 *Interplanetary Dust* (*Astrophysics and Space Science Library*) vol 385, ed Grün E *et al* (Heidelberg: Springer) pp 641–725
[12] Kimura Y 2012 *Nanodust in the Solar System: Discoveries and Interpretations* (*Astrophysics and Space Science Library*) vol 385, ed Mann I *et al* (Heidelberg: Springer) pp 31–46
[13] Weibel E R 1991 *Am. J. Physiol.* **261** 361–9
[14] Lavvas P 2011 *Astrophys. J.* **728** 80
[15] Li A 2004 *Astrophysics of Dust* (*ASP Conference Series*) vol 309, ed Witt A N *et al* (Heidelberg: Springer) pp 417–52
[16] Fitting H-J *et al* 2001 *J. Electron Spectrosc. Relat. Phenom.* **119** 35–47
[17] Vostrikov A A and Dubov D Y 2006 *Tech. Phys.* **51** 1537–52
[18] Megner L and Gumbel J 2009 *J. Atmos. Solar Terr. Phys.* **71** 1236–44
[19] Michaud M and Sanche L 1987 *Phys. Rev.* A **36** 4672–83
[20] Draine B T and Salpeter E E 1979 *Astrophys. J.* **231** 77–94
[21] Pavlů J *et al* 2009 *Contrib. Plasma Phys.* **49** 169–86
[22] Watson W D 1972 *Astrophys. J.* **176** 103–10
[23] Weingartner J C and Draine B T 2001 *Astron. Astrophys. Suppl.* **134** 263–381
[24] Wong K, Vongehr S and Kresin V V 2001 *Phys. Rev.* B **67** 035406
[25] Draine B T and Li A 2001 *Astrophys. J.* **551** 807–24
[26] Meyer-Vernet N 2013 *Icarus* **226** 583–90
[27] Rapp M and Lübken F-J 2001 *J. Atmos. Solar Terr. Phys.* **63** 759–70
[28] Robertson S and Sternovsky Z 2008 *Phys. Plasmas* **15** 040702
[29] Draine B T and Sutin B 1987 *Astrophys. J.* **320** 803–17
[30] Rapp M and Thomas G E 2006 *J. Atmos. Solar Terr. Phys.* **68** 715–44
[31] Gumbel J and Megner L 2009 *J. Atmos. Solar Terr. Phys.* **68** 1225–35
[32] Hill J R and Mendis D A 1979 *Moon Planets* **21** 3–16
[33] Spitzer L Jr 1978 *Physical Processes in the Interstellar Medium* (New-York: Wiley) p 185
[34] Meyer-Vernet N 1984 *Icarus* **57** 422–31
[35] Misconi N Y 1993 *J. Geophys. Res.* **98** 18951–61
[36] Mann I, Meyer-Vernet N and Czechowski A 2014 *Phys. Rep.* **536** 1–39
[37] Whipple E C 1981 *Rep. Prog. Phys.* **44** 1197–250
[38] Grard R J L 1973 *J. Geophys. Res.* **78** 2885–906
[39] Meyer-Vernet N 1982 *Astron. Astrophys.* **105** 98–106
[40] Havnes O, Morfill G E and Goertz C K 1984 *J. Geophys. Res.* **89** 10999–1003
[41] Whipple E C, Northrop T G and Mendis D A 1985 *J. Geophys. Res.* **90** 7405–13
[42] Mendis D A and Rosenberg M 1994 *Annu. Rev. Astron. Astrophys.* **32** 419–63
[43] Hsu H *et al* 2011 *J. Geophys. Res.* **116** A09215
[44] Mendis D A and Axford W I 1974 *Ann. Rev. Earth Planet. Sci.* **2** 419–74
[45] Izmodenov V V 2009 *From the Outer Heliosphere to the Local Bubble* (Space Science Series of ISSI) ed Linsky J L *et al* (New York: Springer) pp 139–50
[46] Slavin J D et al 2010 *Solar Wind 12* (*AIP Conference Proceedings*) vol 1216, ed Maksimovic M *et al* (New York: American Institute of Physics) pp 497–501
[47] Meyer-Vernet N 2007 *Basics of the Solar Wind* (Cambridge: Cambridge University Press) pp 291–9, 337, 347, 339
[48] Czechowski A and Mann I 2012 *Nanodust in the Solar System: Discoveries and Interpretations* (*Astrophysics and Space Science Library*) vol 385, ed Mann I *et al* (Heidelberg: Springer) pp 47–75
[49] Mann I *et al* 2010 *Plasma Phys. Control. Fusion* **52** 124012
[50] Belheouane S 2014 Nanoparticules dans le milieu interplanétaire: observations spatiales et théorie *PhD Thesis* Université Pierre et Marie Curie
[51] Friedrich M and Rapp M 2009 *Surveys Geophys.* **30** 525–59
[52] Havnes O *et al* 1996 *J. Geophys. Res.* **101** 10839–47
[53] Rapp M and Lübken F-J 2004 *Atmos. Chem. Phys.* **4** 2601–33
[54] Carpenter J D *et al* 2007 *J. Geophys. Res.* **112** E08008
[55] Sagdeev R Z *et al* 1989 *Adv. Space Res.* **9** 263–7
[56] Coates A J *et al* 2007 *Geophys. Res. Lett.* **34** L22103
[57] Lavvas P *et al* 2013 *Proc. Natl Acad. Sci.* **110** 2729–34
[58] Jones G H *et al* 2009 *Geophys. Res. Lett.* **36** L16204
[59] Hill T W *et al* 2012 *J. Geophys. Res.* **117** A05209
[60] Grün E *et al* 1992 *Science* **257** 1550–2
[61] Zook H A *et al* 1996 *Science* **274** 1501–3
[62] Meyer-Vernet N *et al* 2009b *Geophys. Res. Lett.* **36** L03103
[63] Kempf S *et al* 2005 *Science* **307** 1274–6
[64] Meyer-Vernet N *et al* 1998 *Measurement Techniques in Space Plasmas: Fields Geophysical Monograph Series*) vol 103, ed Pfaff R *et al* (Washington, DC American Geophysical Union pp 205–10
[65] Meyer-Vernet N 1979 *J. Geophys. Res.* **84** 5373–7
[66] Meyer-Vernet N and Perche C 1989 *J. Geophys. Res.* **94** 2405–15
[67] Meuris P, Meyer-Vernet N and Lemaire J F 1996 *J. Geophys. Res.* **101** 24471–7
[68] Meyer-Vernet N 2001 *Proc. 7th Spacecraft Charging Technology Conf. (The Netherlands, 23–27 April 2001) ESA SP*) vol 476, ed R A Harris (Nordwijk: European Space Agency) pp 635–40
[69] Aubier M G, Meyer-Vernet N and Pedersen B M 1983 *Geophys. Res. Lett.* **10** 5–8
[70] Gurnett D A *et al* 1983 *Icarus* **53** 236–54
[71] Oberc P 1996 *Adv. Space Res.* **17** 105–10
[72] Meyer-Vernet N *et al* 2014 *Geophys. Res. Lett.* **41** 2716–20
[73] Pantellini F *et al* 2012 *Astrophys. Space Sci.* **341** 309–14
[74] Meyer-Vernet N 1985 *Adv. Space Res.* **5** 37–46
[75] Auer S 2001 *Interplanetary Dust* ed Grün E *et al* (Heidelberg: Springer) pp 385–444
[76] Göller J R and Grün E 1989 *Planet. Space Sci.* **37** 1197–206
[77] Burchell M J *et al* 1999 *Meas. Sci. Technol.* **10** 41–50
[78] Price M C *et al* 2012 *Meteorit. Planet. Sci.* **47** 684–95
[79] Pantellini F *et al* 2012 *Plasma Phys. Control. Fusion* **54** 045005
[80] McBride N and McDonnell J A M 1999 *Planet. Space Sci.* **47** 1005–13
[81] Lai S T, Murad E and McNeil W J 2002 *J. Spacecr. Rockets* **39** 106–14

[82] Collette *et al* 2014 *J. Geophys. Res.* **119** 1883–902
[83] Graps A L *et al* 2001 *Proc. Meteoroids Conf. (Kiruna, Sweden, 6–10 August 2001*) (Nordwijk: European Space Agency) pp 601–8
[84] Mann I, Murad E and Czechowski A 2007 *Planet. Space Sci.* **55** 1000–9
[85] Zaslavsky A *et al* 2012 *J. Geophys. Res.* **117** A05102
[86] Le Chat G *et al* 2013 *Solar Phys.* **286** 549–59
[87] Schippers P *et al* 2014 *Geophys. Res. Lett.* **41** 5382–88
[88] Pantellini F *et al* 2013 *Solar Wind 13 (AIP Conf. Proc.)* vol 1539, ed Zank G P *et al* (New York: American Institute of Physics) pp 414–7
[89] Grün E, Zook H A Fechtig H and Giese R H 1985 *Icarus* **62** 244–72
[90] Ceplecha Z *et al* 1998 *Space Sci. Rev.* **84** 327–471
[91] Juhasz A and Horanyi M 2013 *Geophys. Res. Lett.* **40** 2500–4
[92] Mann I and Czechowski A 2012 *Nanodust in the Solar System: Discoveries and Interpretations* (*Astrophysics and Space Science Library*) vol 385, ed Mann I *et al* (Heidelberg: Springer) pp 195–219
[93] Postberg F 2006 *Icarus* **183** 122–34
[94] O'Brien L *et al* 2014 *Rev. Sci. Instrum.* **85** 035113